CHARACTERISTICS OF $MnFe_2O_4$ NANOPARTICLES PREPARED AT HIGH MOLARITY OF CO-PRECIPITATING AGENT NaOH

Sudha Gulati*

Article History: **Received:** 02.11.2021 **Revised:** 29.12.2021 **Accepted:** 11.01.2022

Abstract

$MnFe_2O_4$ nanoparticles were synthesised using co-precipitation method and investigated by the techniques such as x-ray diffraction (XRD), field effect scanning electron microscopy (FESEM) and a vibrating sample magnetometer (VSM). The nanoparticles were of an average crystallite size of ~ 20 nm at molarities 7M and 9M of NaOH without annealing / sintering the samples. X-ray diffraction was used to determine the crystallite size, lattice parameter, and density of the nanoparticles. The FESEM images clearly show the production of spherical nanoparticles. Manganese ferrite nanoparticles were found to have the correct stoichiometry, as is evident from energy-dispersive X-ray spectroscopy (EDS). The saturation magnetization, coercivity, retentivity, squareness ratio, dead layer thickness, magnetic moment, and anisotropy constant were estimated using VSM.

Keywords: Molarity; $MnFe_2O_4$; Coercivity; Saturation magnetisation; Nanoparticles; Co-precipitation

*Department of Physics, Kalindi College, East Patel Nagar, New Delhi – 110008,
email: sudhagulati@kalindi.du.ac.in

DOI: 10.53555/ecb/2022.11.01.22

1 Introduction

Spinel ferrites have been at the frontiers of nanoscience because of their exceptional magnetic, electrical and optical properties [1]. This class of nanomaterials have numerous uses including storage devices, sensors, the production of transformers and inductors, biomedical applications, etc. [2–3]. AB_2O_4 demonstrates the spinel ferrites. Divalent cations A^{2+} (Mn^{2+}, Co^{2+}, Ni^{2+}, etc.) occupy the interstitial tetrahedral places in the formula, while B^{3+} (Fe^{3+}, Mn^{3+}, etc.) occupy the octahedral sites [4]. Various methods such as sol-gel, microemulsion, and hydrothermal, etc. have been used to synthesise ferrites [5 - 7]. The synthesis technique, the substitution of various cations, annealing temperature and time, porosity, crystallite size, chemical composition, and the distribution of cations, etc. affect the properties of ferrites [8 – 10].

In this work, $MnFe_2O_4$ is synthesised by the co-precipitation method as it is a very economical method. The literature survey shows that the pH parameter during synthesis plays a key role in controlling the ferrite nanostructure and its properties [11 - 13]. In the co-precipitation process, the molarity of NaOH determines the pH value used to synthesise ferrite. The effects of pH in the range of 8–12 on the structural and magnetic characteristics of $MnFe_2O_4$ have been researched by Puspitasari et al [11]. It was found that the unsintered particles were amorphous and had saturation magnetisation values of less than 3 emu/g. With a rise in pH, a reduction in particle size was seen. The saturation magnetisation (M_S) was discovered to be 31.36 emu/g for the sample sintered at a temperature of 600°C and a pH value of 11, according to the study by Ahalya et al [12]. With ammonia acting as a co-precipitating agent, Islam et al. reported that sodium hydroxide was unsuitable as a precipitating agent due to the formation of larger particle sizes, which contributed to the non-stable colloidal solution [13]. The particle size and M_S were also reported to increase with an increase in pH. At 300 K and a pH of 12, saturation magnetisation of 66 emu/g has been reported. Trandafir et al. [14] studied the effect of molar concentration of the precipitating agent (NaOH) in the range of 1— 5 M on the properties of zinc ferrite.

When the crystallite size is less than the critical size, the nanoparticles become superparamagnetic in nature. Superparamagnetic nanoparticles are significant for biomedical applications such as heat therapy, cancer diagnostics, treatment, etc., [15 - 16]. No work has been reported on the effects of high molarity (7M, 9M) of NaOH on the properties of superparamagnetic manganese ferrites. In the current work, the structural, morphological, and magnetic properties of superparamagnetic $MnFe_2O_4$ nanoparticles (without annealing /sintering) were studied for high molarity (7M, 9M) of co-precipitating agent NaOH. The samples have been analysed using XRD, FESEM, and VSM techniques.

2. Experimental

2.1 Synthesis of $MnFe_2O_4$ nanoparticles

$MnFe_2O_4$ nanoparticles were produced using the co-precipitation method. $MnCl_2.4H_2O$ and $FeCl_3$ were dissolved in deionized water to obtain 1.0 M and 2.0 M solutions, respectively. The combination of these solutions (labelled as solution a), was heated on a magnetic stirrer at 60°C. NaOH solution was prepared with 7M molarity in deionised water, after that it was boiled, and added to solution a, as a result of which dark brown solution was formed. This brown solution was swirled magnetically at 85°C for two hours, resulting into the formation of dark brown $MnFe_2O_4$ nanoparticles. The resultant product was thoroughly rinsed for 10 times in deionised water to remove unwanted residual of NaCl and finally washed with ethanol. This material was then vacuum dried, and thereafter it was ground with a mill and pestle to prepare dark brown powdered $MnFe_2O_4$ nanoparticles. The aforementioned technique was used to obtain $MnFe_2O_4$ nanoparticles at a molarity of 9M of NaOH. The samples thus prepared for NaOH molar concentrations of 7M and 9M were designated as samples MF7 and MF9 respectively. The chemical reaction for the synthesis of $MnFe_2O_4$ is:

$$MnCl_2 + 2FeCl_3 + 8NaOH \text{ -----> } MnFe_2O_4 + 8NaCl + 4H_2O \quad (1)$$

2.2 Characterization

X-ray diffraction (XRD) analysis was conducted on the Ultima IV utilising CuK_α radiation (=1.5406Å) at 40 kV and 40 mA for the values of 2θ between 10° and 80° to determine phase, crystallite size, lattice parameter, and density. Zeiss Gemini SEM500 with energy-dispersive X-ray spectroscopy was used to examine the morphology, microstructure and elemental composition of the samples. The magnetic measurements were studied using a Physical Properties Measurement System (MicroSense EV9 VSM systems) with a field varying from -10000 Oe to 10000 Oe at room temperature and the estimates were made for the following quantities: squareness ratio ($S=M_r/M_S$), coercivity (H_C), remnant magnetization (M_r),

magnetic moment (μ), and anisotropy constant (K_a).

3 Results and Discussion

3.1 Structural analysis

The X-ray diffraction patterns for the samples MF7 and MF9 of $MnFe_2O_4$ nanoparticles for 2θ ranging from 20° to 70° at room temperature, are presented in Figure 1.

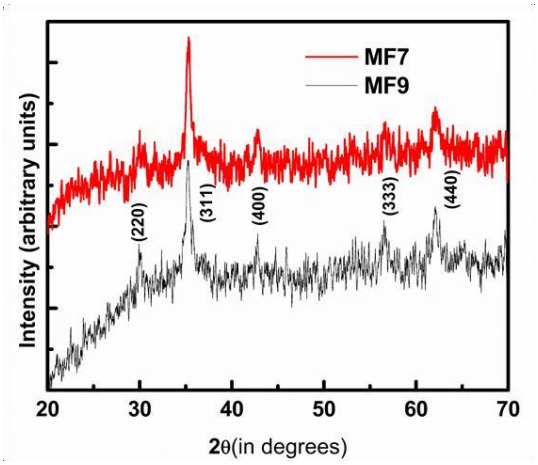

Figure 1: XRD patterns of samples MF7 and MF9.

Figure 1 shows that the peaks coincide well with peaks reported in earlier studies of manganese ferrite and are also in agreement with JCPDS data card (74-2403). The samples showed crystalline nature, the cubic spinel structure with space group Fd3m, and the Bragg diffraction peaks correspond to (220), (311), (400), (333), and (440) phases. The peaks were marked in Figure 1. No peaks were observed in respect of the impurities or secondary phases. The following equations were used to compute the density (ρ), lattice parameter (a), and crystallite size (d) [17 - 19].

$$d = \frac{0.9\,\lambda}{\beta \cos\theta} \qquad (2)$$

$$a = \frac{\lambda \sqrt{h^2 + k^2 + l^2}}{2 \sin\theta} \qquad (3)$$

$$\rho = \frac{8\,M}{N\,a^3} \qquad (4)$$

where (λ =1.5406Å) is the X-ray wavelength, β is the FWHM (full width at half maximum) of the major diffraction peak, θ is the Bragg angle of the strongest peak, (h k l) are plane indices for the greatest intensity peak in the XRD pattern, M is the molecular weight, N is the Avogadro's number, and a^3 is the cubic unit cell volume.

The structural parameters (crystallite size, lattice parameter and density) for the samples MF7 and M9 are listed in Table 1. The values of lattice parameters and density of the samples agree well with JCPDS card 74-2403 and are similar to the reported values [20, 21]. In the present work, the crystallite sizes of the samples MF7 and MF9 were 18.9 nm and 20.3 nm respectively without annealing / sintering the samples. Ahalya et al. reported crystallite size in the range of 26 – 31 nm for the annealed samples prepared at a pH of 8 and 11 [12]. Puspitasari et al. reported crystallite size in the range of 29 nm – 59 nm for the samples prepared at pH of 8, 10 and 12 which were sintered at temperature of 1000 °C for 3h [11].

Table 1 Values of crystallite size (d), lattice parameter (a) and density (ρ) determined from the XRD patterns.

Sample	d (nm)	a (Å)	ρ (g/cc^3)
MF7	18.9	8.424	5.11
MF9	20.3	8.425	5.12

3.2 Morphological Analysis

Figure 2 and Figure 3 display FESEM images and EDS spectra of $MnFe_2O_4$ nanoparticles. The FESEM micrographs showed sphere-shaped nanoparticles and the particles were clumped together which may be attributed to the magnetic interaction among them.

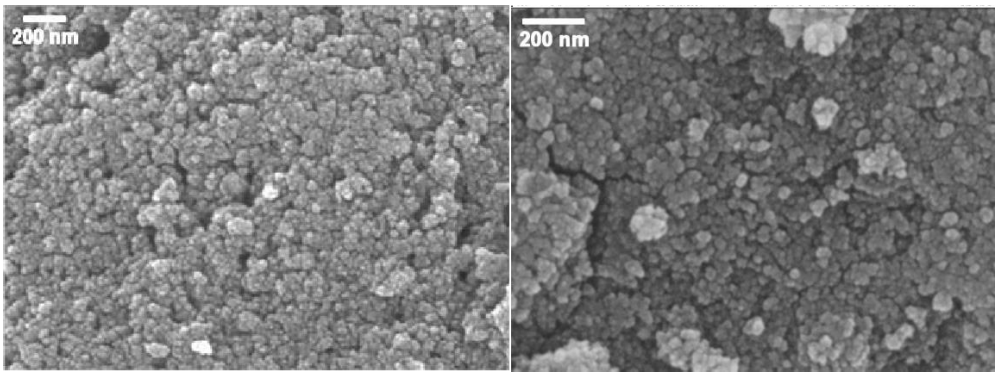

(a) (b)

Figure 2 FESEM images of $MnFe_2O_4$ nanoparticles (a) MF7 and (b) MF9.

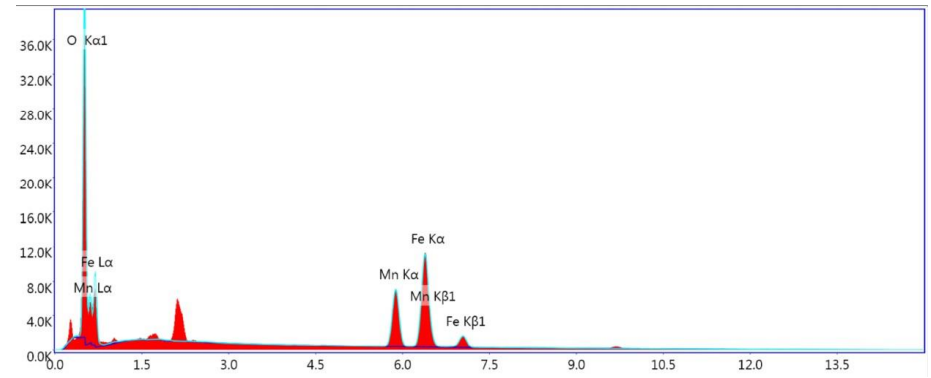

(a)

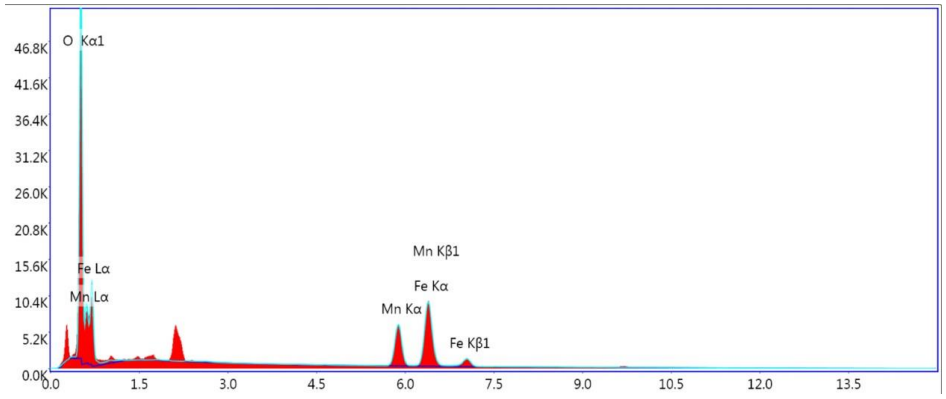

(b)

Figure 3 EDS spectra of $MnFe_2O_4$ nanoparticles (a) MF7, and (b) MF9.

The Energy Dispersive X-ray (EDS) spectra were used to determine the elemental composition of the nanoparticles. The data of weight % and atomic % were depicted in Table 2 and the values of the theoretical and experimental ratios of Mn/Fe and Fe/O were shown in Table 3.

Table 2 Weight % and atomic % of the elements O, Mn, and Fe in samples MF7 and MF9 obtained from EDS analysis.

Element	MF7		MF9	
	Wt%	At%	Wt%	At%
O	20.25	46.85	27.37	56.67
Mn	26.79	18.05	24.97	15.06
Fe	52.96	35.10	47.66	28.27

Table 3 Values of theoretical (theo) and experimental (exp) ratios of Mn/Fe and Fe/O.

Sample	$(Mn/Fe)_{Theo}$	$(Mn/Fe)_{exp}$	$(Fe/O)_{Theo}$	$(Fe/O)_{exp}$
MF7	0.50	0.51	0.5	0.74
MF9	0.50	0.53	0.5	0.5

According to the EDS spectra, elements, namely iron, oxygen, and manganese, were present and there were no signs of contaminants or other substances in the samples. Due to various instrument and process software parameters, such as the data dead time, work distance, acceleration voltage, and acquisition time, the calculated stoichiometric ratios obtained from EDS and the theoretical stoichiometric ratios in these samples may vary. However, in the present work, the measured manganese to iron composition ratios (Mn:Fe) and the iron to oxygen composition ratios (Fe:O) were found to be compatible with the theoretical composition ratios, indicating that the stoichiometry was maintained in the samples.

3.3 Magnetic properties

Hysteresis shapes of $MnFe_2O_4$ nanoparticles were carried out using VSM as shown in Figure 4. The insets show the magnified plots highlighting hysteresis loops at low applied fields.

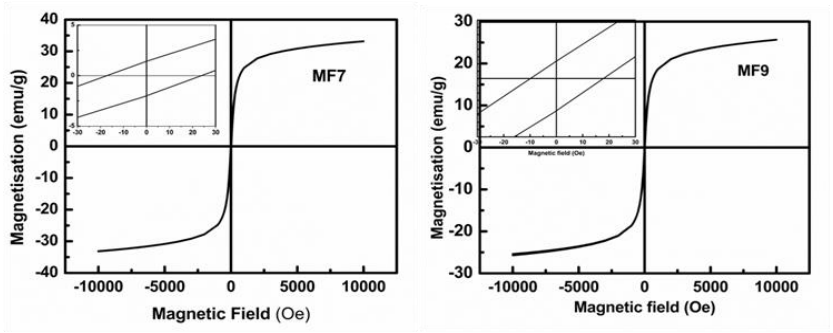

Figure 4 Hysteresis curves of $MnFe_2O_4$ samples (a) MF7 (b)MF9.

The magnetic moment (μ) per formula unit is determined using the equation [22]

$$\mu = \frac{M_s * M}{\mu_B * N_A} \qquad (5)$$

where M_S, N_A, M, μ_B, and are the saturation magnetization, molecular weight, Bohr magnetron and Avogadro's number respectively.

The following relation is used to calculate the magnetic anisotropy constant [23]:

$$k_a = \frac{M_S * H_C}{0.96} \qquad (6)$$

The canting of the surface spins, the formation of a high anisotropy layer or the loss of the long-range order in the surface layer have all been reported to cause the formation of a magnetic dead layer at the surface of magnetic nanoparticles [24]. Equation 7 describes the relationship between the crystallite size of the nanoparticles, M_S, the saturation magnetization of the corresponding bulk material, M_{sb}, and the thickness of the magnetically inactive layer, t [25].

$$M_S = M_{Sb}\ (1 - \frac{6\,t}{d}) \qquad (7)$$

The values of saturation magnetization (M_S), retentivity (M_r), coercivity (H_C), ratio t/d, squareness ($S=M_r/M_S$), magnetic moment (μ), and anisotropy constant (K_a) are presented in Table 4.

The computed values of t/d of the samples shows that M_S declines as t/d was increased. This could be explained by the fact that when the molarity of NaOH increases, the effects of an inactive magnetic layer or a disordered layer on the surface of nanoparticles become more pronounced.

Table 4 Saturation magnetization (M_S), Coercivity (H_C), Retentivity (M_r), squareness (S), magnetic moment (μ), and anisotropy constant (K_a) of $MnFe_2O_4$ samples at room temperature.

Sample	M_s (emu/g)	M_r (emu/g)	H_c (Oe)	$S = M_r/M_s$	μ (μ_B)	k_a (emug^{-1}Oe)	t/d
MF7	33.1	1.69	20.5	0.05	1.36	706	0.098
MF9	25.6	0.88	13.6	0.03	1.05	362	0.113

It has been reported that several variables such as grain size, magnetic particle structure, exchange coupling between collinear spins in the core, canted spins on the surface, etc., influence the coercivity of the nanoparticles[26]. In the $MnFe_2O_4$ samples (MF7 and MF9), the value of coercivity H_C is ~13 Oe. Such kind of substances having low coercivity are beneficial to treat hyperthermia and which could be employed in magnetic recording devices such as hard drives, floppy discs, and videotapes [27].

Table 2 shows that the magnetic moment is proportional to the saturation magnetization M_S, and falls when the molarity of NaOH increases. The decrease in magnetic moment indicates the weakness of the super-exchange interactions among the sites [28].

Rafique et al. reported that the critical diameter of $MnFe_2O_4$ nanoparticle is 42.9 nm, below which the particle shows superparamagnetic nature [29]. Gnanaprakash et al. [30] claim that the particle size limit for $MnFe_2O_4$ particles is 42 nm. In the present work, the $MnFe_2O_4$ particles had crystallite sizes 24.8 and 34.7 nm, which is less than the estimated critical size limit and hence the particles have superparamagnetic characteristics.

Table 2 shows that the magnetic anisotropy constant K_a falls as molarity increases. This might be because there are less Mn^{2+} ions present at the octahedral location with increase in molarity. On the basis of the Stoner-Wohlfarth (S-W) theory,"

the squareness S can have two values, one around 0.83 connected to cubic anisotropy and the other around 0.5 related to uniaxial anisotropy" [31]. Table 2 demonstrates that S has values 0.1 (i.e., 0.5), which are caused by the effects of surface spin disorder. A multi-domain structure with uniaxial anisotropy and incomplete coupling is suggested by values of squareness S (less than 0.5) in the samples.

4 Conclusions

The co-precipitation method was used to prepare the superparamagnetic nanoparticles without annealing / sintering. FESEM images of all the samples demonstrate that they are spherical in shape, have a nano size, are agglomerated and have an appropriate stoichiometry. Crystallite size, lattice constant, and density were determined by analysing the X-ray patterns of $MnFe_2O_4$ nanoparticles. Samples generated with high molarities of NaOH have saturation magnetization values of 33.1 and 25.6 emu/g. The nanoparticles tested were found to be superparamagnetic, with coercivity values of 20.5 and 13.6 Oe and retentivity values of 1.69 and 0.08 emu/g. The ratio t/d is related to saturation magnetization. Further, multi-domain structure along with uniaxial anisotropy and an incomplete coupling is suggested by the values of squareness S (less than 0.5) in the samples.

References

1. Shirsath, S.E., Jadhav, S.S., Toksha, B.G., Patange, S.M. and Jadhav, K.M., 2011. Remarkable influence of Ce4+ ions on the electronic conduction of Ni1− 2xCexFe2O4. *Scripta Materialia, 64*(8), pp.773-776.
2. Anil Kumar, P.S., Shrotri, J.J., Deshpande, C.E. and Date, S.K., 1997. Systematic study of magnetic parameters of Ni–Zn ferrite synthesized by soft chemical approaches. *Journal of applied physics, 81*(8), pp.4788-4790.
3. Soufi, A., Hajjaoui, H., Elmoubarki, R., Abdennouri, M., Qourzal, S. And Barka, N., 2021. Spinel ferrites nanoparticles: Synthesis methods and application in heterogeneous Fenton oxidation of organic pollutants–A review. *Applied Surface Science Advances*, 6, p.100145.
4. Kefeni, K.K., Msagati, T.A. and Mamba, B.B., 2017. Ferrite nanoparticles: synthesis, characterisation and applications in electronic device. *Materials Science and Engineering: B, 215*, pp.37-55.
5. Khan, H., 2019. Effective heterogeneous photocatalytic degradation of crystal violet dye using manganese ferrite nanoparticles. *Pakistan Journal of Analytical & Environmental Chemistry, 20(1)*, pp.32-38.
6. Li, M., Gao, Q., Wang, T., Gong, Y.S., Han, B., Xia, K.S. and Zhou, C.G., 2016. Solvothermal synthesis of MnxFe3− xO4 nanoparticles with interesting physicochemical characteristics and good catalytic degradation activity. *Materials & Design, 97*, pp.341-348, DOI: 10.1016/j. matdes.2016.02.103.
7. Wang, G., Zhao, D., Kou, F., Ouyang, Q., Chen, J. and Fang, Z., 2018. Removal of norfloxacin by surface Fenton system (MnFe2O4/H2O2): kinetics, mechanism and degradation pathway. Chemical Engineering Journal, 351, pp.747-755, DOI: 10.1016/j.cej.2018.06.033.
8. Wang, Z., Liu, J., Li, T., Liu, J. and Wang, B., 2014. Controlled synthesis of MnFe 2 O 4 nanoparticles and Gd complex-based nanocomposites as tunable and enhanced T 1/T 2-weighted MRI contrast agents. *Journal of Materials Chemistry B, 2*(29), pp.4748-4753, DOI: 10.1039/C4TB00342J.
9. Kwon, J., Kim, J.H., Kang, S.H., Choi, C.J., Rajesh, J.A. and Ahn, K.S., 2017. Facile hydrothermal synthesis of cubic spinel AB2O4 type MnFe2O4 nanocrystallites and their electrochemical performance. *Applied Surface Science, 413*, pp.83-91, DOI: 10.1016/j.apsusc.2017.04.022.
10. Yadav, R.S., Kuřitka, I., Vilcakova, J., Jamatia, T., Machovsky, M., Skoda, D., Urbánek, P., Masař, M., Urbánek, M., Kalina, L. and Havlica, J., 2020. Impact of sonochemical synthesis condition on the structural and physical properties of MnFe2O4 spinel ferrite nanoparticles. *Ultrasonics sonochemistry, 61*, p.104839., DOI: 10.1016/j.ultsonch.2019.104839.
11. Puspitasari, P., Muhammad, A. and Suryanto, H., 2018. Determination of the magnetic properties of manganese ferrite by the coprecipitation method at different pH concentrations. *High Temperature Material Processes: An International Quarterly of High-Technology Plasma Processes, 22*(4).
12. Ahalya, K., Suriyanarayanan, N. and Sangeetha, S., 2014. Effect of pH and annealing temperatures on structural, magnetic, electrical, dielectric and adsorption properties of manganese ferrite nano particles. *Materials science in semiconductor processing, 27*, pp.672-681.

13. Islam, K., Haque, M., Kumar, A., Hoq, A., Hyder, F. and Hoque, S.M., 2020. Manganese ferrite nanoparticles (MnFe2O4): Size dependence for hyperthermia and negative/positive contrast enhancement in MRI. *Nanomaterials*, *10*(11), p.2297.
14. Trandafir, E.V., Ciocarlan, R., Pui, A., Hempelmann, R. And Caltun, O.F., 2020. Influence of Precipitating Agent Concentration on Nanoparticles Size and Magnetic Properties of Zinc Ferrites, DOI: 10.37358/RC.20.2.7878.
15. Kanagesan, S., Aziz, S.B.A., Hashim, M., Ismail, I., Tamilselvan, S., Alitheen, N.B.B.M., Swamy, M.K. and Purna Chandra Rao, B., 2016. Synthesis, characterization and in vitro evaluation of manganese ferrite (MnFe2O4) nanoparticles for their biocompatibility with murine breast cancer cells (4T1). Molecules, 21(3), p.312.
16. Hussain, S.M., Javorina, A.K., Schrand, A.M., Duhart, H.M., Ali, S.F. and Schlager, J.J., 2006. The interaction of manganese nanoparticles with PC-12 cells induces dopamine depletion. *Toxicological sciences*, *92*(2), pp.456-463.
17. Roni, M.M., Hoque, K., Paul, T.C., Khan, M.N.I. and Hossain, M.E., 2021. Synthesis of La-doped Mn0· 6Zn0. 4LaxFe2-xO4 and the study of its structural, electrical and magnetic properties for high frequency applications. *Results in Materials*, *11*, p.100215.
18. Alonizan, N.H. and Qindeel, R., 2018. Structural and magnetic properties of ytterbium substituted spinel ferrites. *Applied Physics A*, *124*, pp.1-7.
19. Kurmude, D.V., Barkule, R.S., Raut, A.V., Shengule, D.R. and Jadhav, K.M., 2014. X-ray diffraction and cation distribution studies in zinc-substituted nickel ferrite nanoparticles. *Journal of Superconductivity and Novel Magnetism*, *27*, pp.547-553.
20. Kurtinaitiene, M., Mazeika, K., Ramanavicius, S., Pakstas, V. and Jagminas, A., 2016. Effect of additives on the hydrothermal synthesis of manganese ferrite nanoparticles. *Advances in Nano Research*, *4*(1), p.1.
21. Pande, S., Islam, M.M., Mohanta, S.C. and Uddin, N., 2019. Single-step synthesis of manganese ferrite nanoparticles with enhanced magnetization via chemical co-precipitation route. *Journal of Scientific Research*, *11*(2), pp.225-234.
22. Nikmanesh, H., Kameli, P., Asgarian, S.M., Karimi, S., Moradi, M., Kargar, Z., Ventura, J., Bordalo, B. and Salamati, H., 2017. Positron annihilation lifetime, cation distribution and magnetic features of Ni 1− x Zn x Fe 2− x Co x O 4 ferrite nanoparticles. *RSC Advances*, *7*(36), pp.22320-22328.
23. Lin, Q., He, Y., Xu, J., Lin, J., Guo, Z. and Yang, F., 2018. Effects of Al3+ substitution on structural and magnetic behavior of CoFe2O4 ferrite Nanomaterials. *Nanomaterials*, *8*(10), p.750.
24. Maehara, T., Konishi, K., Kamimori, T., Aono, H., Hirazawa, H., Naohara, T., Nomura, S., Kikkawa, H., Watanabe, Y. and Kawachi, K., 2005. Selection of ferrite powder for thermal coagulation therapy with alternating magnetic field. *Journal of materials science*, *40*, pp.135-138.
25. El-Sayed, H.M., Ali, I.A., Azzam, A. and Sattar, A.A., 2017. Influence of the magnetic dead layer thickness of Mg-Zn ferrites nanoparticle on their magnetic properties. *Journal of Magnetism and Magnetic Materials*, *424*, pp.226-232.
26. Kolhatkar, A.G., Jamison, A.C., Litvinov, D., Willson, R.C. and Lee, T.R., 2013. Tuning the magnetic properties of nanoparticles. *International journal of molecular sciences*, *14*(8), pp.15977-16009.
27. Hedayatnasab, Z., Abnisa, F. and Daud, W.M.A.W., 2017. Review on magnetic nanoparticles for magnetic nanofluid hyperthermia application. *Materials & Design*, *123*, pp.174-196.
28. Kumar, G., Shah, J., Kotnala, R.K., Singh, V.P., Garg, G., Shirsath, S.E., Batoo, K.M. and Singh, M., 2015. Superparamagnetic behaviour and evidence of weakening in super-exchange interactions with the substitution of Gd3+ ions in the Mg–Mn nanoferrite matrix. *Materials Research Bulletin*, *63*, pp.216-225.
29. Rafique, M.Y., Pan, L.Q., Iqbal, M.Z., Qiu, H.M., Farooq, M.H., Guo, Z.G. and Tanveer, M., 2013. Growth of monodisperse nanospheres of MnFe2O4 with enhanced magnetic and optical properties. *Chinese Physics B*, *22*(10), p.107101.
30. Gnanaprakash, G., Philip, J. and Raj, B., 2007. Effect of divalent metal hydroxide solubility product on the size of ferrite nanoparticles. *Materials Letters*, *61*(23-24), pp.4545-4548.
31. Dimitropoulos, P.D., Stamoulis, G.I. and Hristoforou, E., 2006. A 3-D hybrid Jiles-Atherton/Stoner-Wohlfarth magnetic hysteresis model for inductive sensors and actuators. *IEEE Sensors Journal*, *6*(3), pp.721-736.